- SUPPLEMENTARY INFORMATION -

Interactions between hippocampal activity and striatal dopamine in people at clinical high risk for psychosis: relationship to adverse outcomes

Gemma Modinos, Anja Richter, Alice Egerton, Ilaria Bonoldi, Matilda Azis, Mathilde Antoniades, Matthijs Bossong, Nicolas Crossley, Jesus Perez, James M. Stone, Mattia Veronese, Fernando Zelaya, Anthony A Grace, Oliver D Howes, Paul Allen, Philip McGuire

Supplementary Methods

pCASL acquisition and preprocessing

Parameters for data acquisition were identical for both pCASL datasets, reported previously by our group [1,2]. Subjects were scanned at a General Electric Signa HDX 3.0T scanner with their eyes open, using an 8-channel phased array head coil at the Department of Neuroimaging, Institute of Psychiatry, Psychology and Neuroscience. A high-resolution T2-weighted Fast Spin Echo (FSE) image (TE=54.58ms, TR=4380ms, flip angle 90°, field of view=240) was acquired for image registration.

Pseudo-Continuous Arterial Spin Labelling (pCASL) scans were acquired with a 3D FSE spiral multi-shot readout, after a post-labelling delay of 1.5 s. Parameters of the image readout were as follows: TE=32 ms, TR=5500 ms, spatial resolution of 1x1 mm in plane, 60 slices of 3 mm thickness and three pairs of tagged-untagged images were collected. To maximize the sensitivity to blood perfusion, suppression of the background static tissue signal was achieved by selective saturation of the image slab at 4.3s before acquisition, selective inversion 3 s before acquisition and non-selective inversions at 1.5 s, 764 ms, 334 ms and 84 ms before imaging. Calibration images were collected with the same imaging sequence and were used to quantify blood flow in physiological units (ml blood/100 gm tissue/min).

The sensitivity of the image to water was calibrated at each voxel [3-5]. A low-resolution sensitivity map was created by using a neighbourhood maximum algorithm to avoid regions with partial volume of suppressed fluid. With this co-registered sensitivity map C, cerebral blood flow (CBF) was calculated following the guidelines reported by Alsop et al [4]. The whole ASL pulse sequence, including the acquisition of calibration images, was performed in 6:08 minutes.

FSL (FMRIB Software Library, http://www.fmrib.ox.a.c.uk/fsl) and Statistical Parametric Mapping (SPM12; http://www.fil.ion.ucl.ac.uk/spm/) were used to preprocess CBF maps. The following steps were applied: (1) extra-cerebral signal was removed from the T2 scan using the "Brain Extraction Tool" (BET) of FSL28 and the resulting skull-stripped T2 volume and its corresponding T2 binary mask were then co-registered to the ASL scan; (2) extra-cerebral signal was then eliminated from the CBF map by multiplying it with the co-registered binary brain mask; (3) the skull-stripped CBF map was co-registered back to the space of the original T2 scan to return to their original frame of reference; (4) the T2 and the multiplied ASL scans (step 2) were normalized to SPM's T2 template; (5) the normalized individual CBF map was spatially smoothed using a 6mm Gaussian smoothing kernel.

PET acquisition and preprocessing

The two PET datasets had been reported previously by our group [6,7]. Participants were asked to refrain from eating, drinking (except water), and alcohol consumption for 12h prior to the scan, and from smoking for 2h prior to the scan [8]. One hour before the scan, all participants received 400 mg of entacapone, a peripheral catechol-*o*-methyl-transferase inhibitor, and 150 mg of carbidopa, a peripheral aromatic acid decarboxylase inhibitor. Participants were positioned in the scanner with the orbitomeatal line parallel to the transaxial plane of the tomograph. To correct for attenuation, the head position was marked and monitored, and a CT scan was conducted. Thirty seconds after the start of the dynamic PET scan, approximately 150 MBq of ^{18}F-DOPA was administered by bolus intravenous injection. PET data were acquired in 32 frames of increasing duration and the whole scan was performed in 95 min (frame intervals: 8x15, 3x60, 5x120, 16x300s).

In terms of image preprocessing, a mutual information algorithm was used to correct for head movement [9]. SPM8 was used to automatically normalise a tracer-specific ^{18}F-DOPA template [10]. A striatal brain atlas using the definition described by Martinez et al. was applied, which includes dividing the striatum into a limbic, associative and sensorimotor subdivision, respectively, based on the predominant origin of projections to the striatum [11].

Exploratory analysis of rCBF x whole striatal dopamine synthesis capacity by hippocampal subfields

Previous studies suggest that perfusion abnormalities in CHR individuals may be particularly evident in the CA1 subregion of the hippocampus [12-14]. For completeness, we examined the relationship between hippocampal rCBF and striatal dopamine synthesis capacity in the CHR-Good compared to CHR-Poor subgroup in SPM12, using analogous procedures to those described for our main analysis. Separate masks for bilateral CA1, CA2, CA3, dentate gyrus, and subiculum were anatomically defined using the cytoarchitectonic probabilistic atlas [15] in the SPM Anatomy toolbox [16] (Figure S2) and used for small volume correction (SVC) in an ANCOVA in SPM12 with the rCBF maps by functional outcome subgroup, individual dopamine (K_i^{cer}) values as regressors, and including age, sex and mean global CBF as covariates of no interest. No further manual editing and/or subfield parcellation accuracy checking was implemented in addition to the automated toolbox routine. For completeness, in this same design we also examined whether rCBF between the CHR-Good and CHR-Poor groups differed by hippocampal subfield. As in our main analyses, we used a voxel-wise height threshold of family-wise error (FWE) correction of $p<0.05$ after small volume correction (SVC) with the pre-defined hippocampal ROI mask.

Supplementary analysis of other CHR clinical outcomes

Transition / non-transition to psychosis
The relationship between hippocampal rCBF and whole striatal dopamine synthesis capacity (K_i^{cer}, min^{-1}) by psychosis transition/non-transition outcome groups was examined using SPM12, dividing the CHR sample into two groups: CHR individuals who developed a psychotic disorder during follow-up period (CHR-T), and those who did not (non-transitioned, CHR-NT). Individual K_i^{cer} values were entered as regressors in a voxel-wise ANCOVA to examine between- and within-group associations of whole striatal dopamine synthesis capacity with hippocampal rCBF in CHR-T compared to CHR-NT individuals. Age, sex and mean global CBF were included as covariates of no interest in the ANCOVA. In addition, exploratory analyses were conducted using measures of dopamine function in striatal subdivisions (limbic, associative and sensorimotor). First, we assessed group differences in dopamine function by striatal subdivision using a multivariate GLM in SPSS. Second, we assessed group interactions on the relationship between dopamine synthesis capacity by striatal subdivision and hippocampal rCBF in SPM12, using the same procedures as in the main interaction analysis. Third, we tested the relationship between hippocampal rCBF and dopamine synthesis capacity in SPM12 using separate masks for the bilateral CA1, CA2, CA3, dentate gyrus, and subiculum. A significance threshold of $p_{fwe}<0.05$ was used for all SPM12 analyses.

CHR remission / non-remission
Based on previous research [17], we also analyzed for completeness the relationship between hippocampal rCBF and whole striatal dopamine synthesis capacity (K_i^{cer}, min^{-1}) by remission/non-remission outcome groups. This was examined in SPM12, by allocating CHR subjects to either

remission (CHR-R, no longer meeting CHR criteria with the Comprehensive Assessment of At-Risk Mental States (CAARMS [18]) or non-remission (CHR-NR, meeting CHR or psychosis criteria) groups on follow-up assessment. We used the same procedures as in the main hippocampal rCBF x striatal dopamine synthesis capacity (K_i^{cer}, min^{-1}) interaction analysis by functional outcome subgroups and above for CHR-T vs CHR-NT: individual K_i^{cer} values were entered as regressors in a voxel-wise ANCOVA to examine between- and within-group associations of whole striatal dopamine synthesis capacity with hippocampal rCBF in CHR-R compared to CHR-NR individuals, including age, sex and mean global CBF as covariates of no interest. In additional exploratory analyses, group differences in (1) dopamine function by striatal subdivision were investigated using a multivariate GLM in SPSS, (2) group interactions on the relationship between dopamine synthesis capacity by striatal subdivision and hippocampal rCBF were examined in SPM12, (3) group interactions on the relationship between whole striatal dopamine synthesis capacity rCBF by hippocampal subfields (bilateral CA1, CA2, CA3, dentate gyrus, and subiculum). A significance threshold of $p_{fwe}<0.05$ was used for all SPM12 analyses.

Supplementary Results

Relationship between hippocampal rCBF and dopamine synthesis capacity by striatal subdivision

Within the CHR-Poor group, hippocampal rCBF was negatively associated with dopamine synthesis capacity in the associative (xyz: 38, -8, -24; k=27; t=4.32, z=3.92, p_{fwe} = 0.005) and limbic striatum (xyz: 28, -6, -28; k=59; t=3.67, z=3.40, p_{fwe} = 0.027), but only at trend level in the sensorimotor striatum (xyz: 38, -8, -24; k=2; t=3.11, z=2.93, p_{fwe} = 0.099). These associations were absent in the CHR-Good group. Group interaction analyses showed that the relationship between hippocampal rCBF and dopamine synthesis capacity in the associative striatum was significantly different between CHR groups (xyz: 40, -12, -24; k=8; t=3.45, z=3.22, p_{fwe} = 0.046), as well as in the sensorimotor striatum (xyz: 40, -12, -24; k=9; t=3.55, z=3.31, P_{FWE} = 0.036), while the group interaction was evident as a strong trend in the limbic striatum (xyz: 34, -10, -26; k=53; t=3.38, z=3.16, p_{fwe} = 0.054) (Figure S5).

Exploratory analysis of rCBF x whole striatal dopamine synthesis capacity by hippocampal subfields

Analysis by hippocampal subfields revealed that the interaction between whole striatal dopamine synthesis capacity, group (CHR-Good vs CHR-Poor) and hippocampal rCBF was significant in the right CA1 subregion (xyz 38, -12, -24, k=6, t=3.24, z=3.05, p_{fwe} = 0.042). This was driven by a significant negative association in CHR individuals with poor functional outcomes (xyz: 38, -12, -24; k=21; t=3.42, z=3.20, p_{fwe} = 0.027), which was absent in CHR individuals with good outcomes. No other significant effects were found in other subfields (CA2, CA3, dentate gyrus and subiculum).

Separate analyses of between-group differences in only rCBF, by hippocampal subfield showed elevated rCBF in the right CA1 subregion in CHR-Poor individuals compared to CHR-Good (xyz: 38, -12, -24; k=15; t=3.37, z=3.16, p_{fwe} = 0.031). No other significant effects were found in other subfields (CA2, CA3, dentate gyrus and subiculum).

Supplementary analyses of other CHR outcomes

Transition / non-transition to psychosis

Of the 50 CHR individuals with available clinical follow-up, six developed a psychotic disorder during follow-up period (CHR-T) and 44 did not (CHR-NT). No significant differences were found in demographic or clinical variables (including medication or cannabis use) at baseline between these groups. Of the 6 CHR-T individuals, five were naïve to antipsychotic or antidepressant medication (1 was taking antidepressants). Of the 44 CHR-NT individuals, 26 were naïve to antipsychotic or antidepressant medication (3 were taking antipsychotics, 15 antidepressants).

Relationship between hippocampal rCBF and striatal dopamine

There was no significant group interaction between rCBF, whole striatal dopamine synthesis capacity and group in the hippocampus (p_{fwe} > 0.05).

While there were no significant between-group differences in total hippocampal rCBF, there was a significant increase in rCBF in the left subiculum in CHR-T compared to CHR-NT (xyz: -24, -22, -26; k=17; t=3.21, z=3.03, p_{fwe} = 0.039). No other significant interaction by hippocampal subfield was found (p_{fwe} > 0.05). There were no significant differences between the two groups in striatal dopamine

synthesis capacity in the whole striatum (F([1,48] = 0.470; p = 0.496; adjusted for age and sex F[1,46] = 0.854, p = 0.360) or by striatal subdivisions (Table S4).

Exploratory analysis of hippocampal rCBF x dopamine synthesis capacity by striatal subdivision
There was a significant group interaction between rCBF in the hippocampus and dopamine synthesis capacity in the associative striatum (xyz: -20, -22, -18; k=112; t=3.76, z=3.48, p_{fwe} = 0.021), which was driven by a positive association in the CHR-T subgroup (xyz: -20, -22, -18; k=128; t=3.89, z=3.58, p_{fwe} = 0.015). There were no significant interactions for any of the other subdivisions (limbic or sensorimotor, p_{fwe} > 0.05).

Exploratory analysis of rCBF x whole striatal dopamine synthesis capacity by hippocampal subfields
Analysis by hippocampal subfields showed a significant interaction between rCBF, whole striatal dopamine synthesis capacity and group (CHR-T vs CHR-NT) in the left subiculum (xyz: -22, -28, -16; k=87; t=3.28, z=3.08, p_{fwe} = 0.034), which was driven by a significant positive association in the CHR-T subgroup (xyz: -20, -24, -18; k=76; t=3.35, z=3.14, p_{fwe} = 0.029). There were no significant interactions with other hippocampal subfields (CA1, CA2, CA3, dentate gyrus, p_{fwe} > 0.05).

CHR remission / non-remission
Sixteen CHR individuals were in remission (CHR-R), and 33 individuals still met CHR criteria (non-remission, CHR-NR) at the follow-up assessment. There were no significant differences between CHR-R and CHR-NR subgroups in terms of age, sex, estimated premorbid IQ, cannabis use, and level of overall functioning. CHR individuals with persistent CHR status (CHR-NR) had significantly higher positive symptoms at baseline (mean: 9.21, SD = 3.35) compared to CHR-R (mean: 5.94, SD = 3.62; df=47, p = 0.003). Of the 16 CHR-R individuals, nine were naïve to antipsychotic or antidepressant medication (2 were taking antipsychotic medication, 5 antidepressant medication). Of the 33 CHR-NR individuals, 21 were naïve to antipsychotic or antidepressant medication (1 was taking antipsychotic medication, 11 antidepressant medication).

Relationship between hippocampal rCBF and striatal dopamine
There was no significant group interaction between rCBF, whole striatal dopamine synthesis capacity and group in the hippocampus (p_{fwe} > 0.05).

When analyzed separately, there were no significant differences between the CHR-R and CHR-NR subgroups in either total hippocampal rCBF or by hippocampal subfield (P_{FWE} > 0.05), striatal dopamine synthesis capacity in the whole striatum (F([1,47] = 0.115; p = 0.736; adjusted for age and sex F[1,45] = 0.493, p = 0.486) or by striatal subdivisions (Table S4).

Exploratory analysis of hippocampal rCBF x dopamine synthesis capacity by striatal subdivision
There were no significant group interactions between rCBF in the hippocampus and striatal dopamine synthesis capacity in any subdivisions (associative, limbic or sensorimotor, p_{fwe} > 0.05).

Exploratory analysis of rCBF x whole striatal dopamine synthesis capacity by hippocampal subfields
There were no significant group interactions between whole striatal dopamine synthesis capacity and rCBF in any hippocampal subfields (CA1, CA2, CA3, dentate gyrus, subiculum, p_{fwe} > 0.05).

Supplementary Tables

Table S1. Baseline characteristics of the first sample (NEUTOP).

	HC (n=16)	CHR (n=45)	HC vs CHR		CHR-Good (n=15)	CHR-Poor (n=19)	CHR-Good vs CHR-Poor	
			T or χ^2	p			T or χ^2	p
Age in years, mean (SD)	25.32 (4.46)	22.92 (3.90)	2.04	0.05	21.46 (2.93)	23.92 (4.02)	-1.99	0.06
Sex (male), N	7 (43.8%)	27 (60%)	1.26	0.26	8	13	0.81	0.37
Years of education, mean (SD)	15.38 (3.96)	14.39 (2.36)	1.19	0.24	14.27 (2.38)	14.11 (2.49)	0.19	0.85
Premorbid IQ estimate	99.93 (12.35)	105.84 (11.50)	-1.58	0.13	104.71 (9.82)	107.61 (12.28)	-0.72	0.48
GAF, mean (SD)	91.84 (5.06)	58.46 (9.10)	17.99	<0.001	56.93 (9.17)	57.00 (9.64)	-0.02	0.98
CAARMS Total, mean (SD)	n/a	42.41 (20.68)	-	-	42.73 (20.17)	43.83 (21.92)	0.63	0.88
CAARMS Positive, mean (SD)	n/a	8.66 (3.64)	-	-	8.80 (3.93)	8.79 (3.72)	0.01	0.99
CAARMS Negative, mean (SD)	n/a	5.83 (3.91)	-	-	6.53 (4.22)	5.50 (3.67)	0.75	0.46
Antipsychotics, N	-	4 (8.9%)	-	-	2 (13.3%)	0	2.69	0.10
Antidepressants, N	-	15 (33%)	-	-	6	6	0.26	0.61
Cannabis use, N	7	19	0.01	0.92	8	7	0.93	0.34

CAARMS, Comprehensive Assessment of At Risk Mental State; CHR, clinical high risk; GAF, Global Assessment of Function; HC, healthy controls; NART, National Adult Reading Test; SD, standard deviation.

Table S2. Baseline characteristics of the second sample (PROD).

	HC (n=12)	CHR (n=22)	HC vs CHR		CHR-Good (n=10)	CHR-Poor (n=6)	CHR-Good vs CHR-Poor	
			T or χ^2	p			T or χ^2	p
Age in years, mean (SD)	23.25 (4.29)	22.55 (4.93)	0.42	0.68	23.30 (6.26)	23.17 (4.01)	0.05	0.96
Sex (male), N	9 (75.0%)	13 (59.1%)	0.86	0.35	7 (70.0%)	2 (33.3%)	2.05	0.15
Years of education, mean (SD)	14.75 (1.22)	13.14 (2.40)	2.60	0.01	13.50 (2.37)	12.33 (2.88)	0.88	0.39
Premorbid IQ estimate	106.83 (10.13)	106.31 (9.36)	0.15	0.88	107.54 (10.78)	108.90 (6.60)	-0.28	0.79
GAF, mean (SD)	83.17 (10.06)	58.00 (9.85)	7.01	<0.001	60.50 (12.14)	56.57 (7.76)	0.69	0.50
CAARMS Total, mean (SD)	n/a	39.81 (12.78)	-	-	36.30 (13.22)	41.67 (10.93)	-0.84	0.42
CAARMS Positive, mean (SD)	n/a	6.68 (3.12)	-	-	5.40 (2.84)	8.17 (3.76)	-1.68	0.12
CAARMS Negative, mean (SD)	n/a	6.00 (3.15)	-	-	5.30 (3.47)	6.50 (3.15)	-0.69	0.50
Antipsychotics, N	-	1 (4.6%)	-	-	1 (10%)	0	0.64	0.42
Antidepressants, N	-	5 (22.7%)	-	-	2	2	0.36	0.55
Cannabis use, N	8	15	0.07	0.79	6	3	0.15	0.70

CAARMS, Comprehensive Assessment of At Risk Mental State; CHR, clinical high risk; GAF, Global Assessment of Function; HC, healthy controls; NART, National Adult Reading Test; SD, standard deviation.

Table S3. Clinic-demographic details of CHR participants with and without clinical follow-up.

	Sample with follow-up (n=50)	Lost to follow-up (n=17)	Sample with vs without follow-up	
			T or χ^2	P
Age in years, mean (SD)	22.97 (4.28)	22.29 (4.14)	0.57	0.57
Sex (male), N	30 (60%)	10 (58.8%)	0.01	0.93
Years of education, mean (SD)	13.82 (2.48)	14.44 (2.26)	-0.95	0.35
Premorbid IQ estimate	106.91 (10.50)	103.41 (11.33)	1.16	0.25
GAF, mean (SD)	57.64 (9.67)	60.41 (7.80)	-1.04	0.30
CAARMS Total, mean (SD)	41.00 (18.04)	43.36 (19.84)	0.43	0.68
CAARMS Positive, mean (SD)	8.04 (3.77)	7.88 (2.99)	0.16	0.87
CAARMS Negative, mean (SD)	5.90 (3.68)	5.86 (3.68)	0.04	0.97
Antipsychotics, N	3 (6%)	2 (11.8%)	0.61	0.44
Antidepressants, N	16 (32%)	4 (24%)	0.44	0.51
Cannabis use, N	24 (48.0%)	10 (58.8%)	0.60	0.44
Global rCBF, mean (SD)	439.54 (89.87)	458.59 (81.94)	-0.77	0.44
Striatal K_i^{cer}, mean (SD)	0.0129 (0.001)	0.0125 (0.001)	0.71	0.20

Abbreviations: CAARMS, Comprehensive Assessment of At Risk Mental State; CHR, clinical high risk; GAF, Global Assessment of Function; SD, standard deviation.

Table S4. Analysis of potential confounding effects of current cannabis use.

Tests of Between-Subjects Effects

Dependent Variable: Hippocampus_rCBFxDA

Source	Type III Sum of Squares	df	Mean Square	F	Sig.
Corrected Model	191353.89[a]	5	38270.778	29.020	.000
Intercept	182.866	1	182.866	.139	.711
Age	790.552	1	790.552	.599	.443
Sex	.806	1	.806	.001	.980
Global_rCBF	152778.636	1	152778.636	115.847	.000
Cannabis_use_current	912.399	1	912.399	.692	.410
Group_GAF	6425.614	1	6425.614	4.872	.033
Error	58026.880	44	1318.793		
Total	4396776.73	50			
Corrected Total	249380.772	49			

a. R Squared = .767 (Adjusted R Squared = .741)

A univariate ANCOVA in SPSS with the individual values from the significant loci of group interaction (cluster average) between hippocampal rCBF and striatal dopamine as dependent variable, Group (CHR-Good vs CHR-Poor) as between-subjects factor, and age, sex, global rCBF and current cannabis use as covariates showed that the group effect remained significant ($F[1,44]=4.872$, $p = 0.033$).

Table S5. Group differences in dopamine synthesis capacity by striatal subdivision.

HC (n=28) vs CHR (n=67)

	F	*p*	F*	*p**
Associative striatum	0.599	0.441	0.384	0.537
Limbic striatum	0.104	0.748	0.168	0.683
Sensorimotor striatum	0.602	0.440	0.376	0.541

*Adjusted for age and gender.

CHR-Good (n=25) vs CHR-Poor (n=25)

	F	*p*	F*	*p**
Associative striatum	2.905	0.095	1.958	0.168
Limbic striatum	3.217	0.079	2.420	0.127
Sensorimotor striatum	0.821	0.372	0.218	0.643

*Adjusted for age and gender.

CHR-NT (n=44) vs CHR-T (n=6)

	F	*p*	F*	*p**
Associative striatum	0.700	0.407	1.138	0.292
Limbic striatum	0.236	0.630	0.333	0.567
Sensorimotor striatum	0.003	0.960	0.089	0.767

*Adjusted for age and gender.

CHR-R (n=33) vs CHR-NR (n=16)

	F	*p*	F*	*p**
Associative striatum	0.010	0.919	0.252	0.618
Limbic striatum	1.734	0.194	2.361	0.131
Sensorimotor striatum	0.024	0.878	0.024	0.878

*Adjusted for age and gender.

Supplementary Figures

Figure S1. Region-of-interest mask for the bilateral hippocampus (green) overlaid on (A) a standard brain template, and (B) a representative subject-level cerebral blood flow map in normalized space.
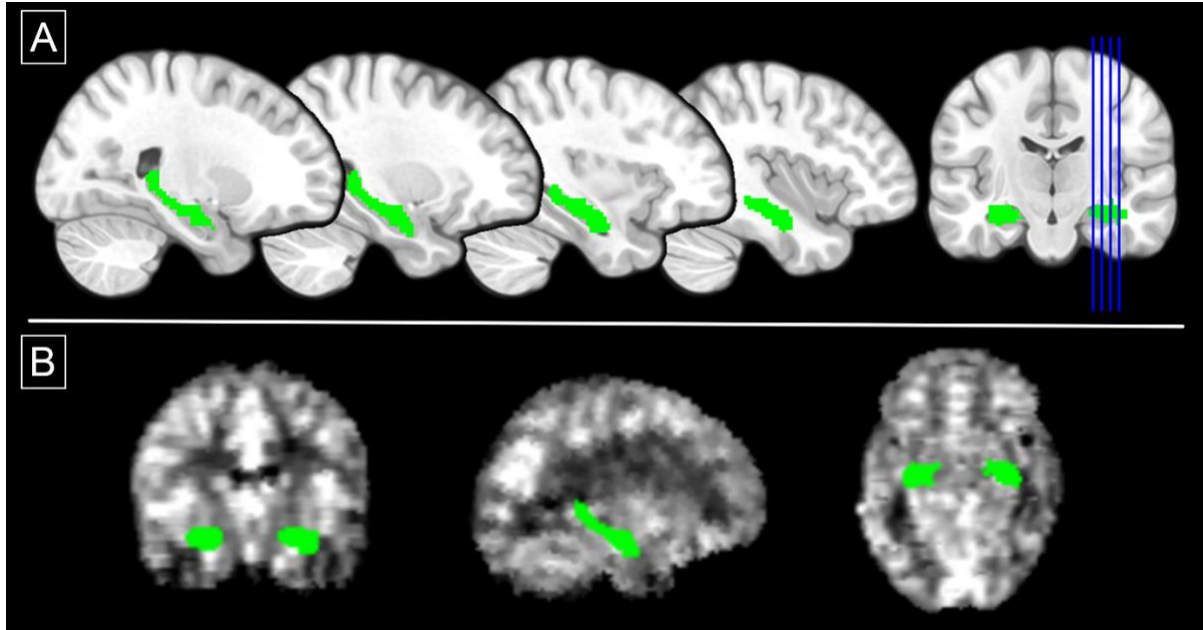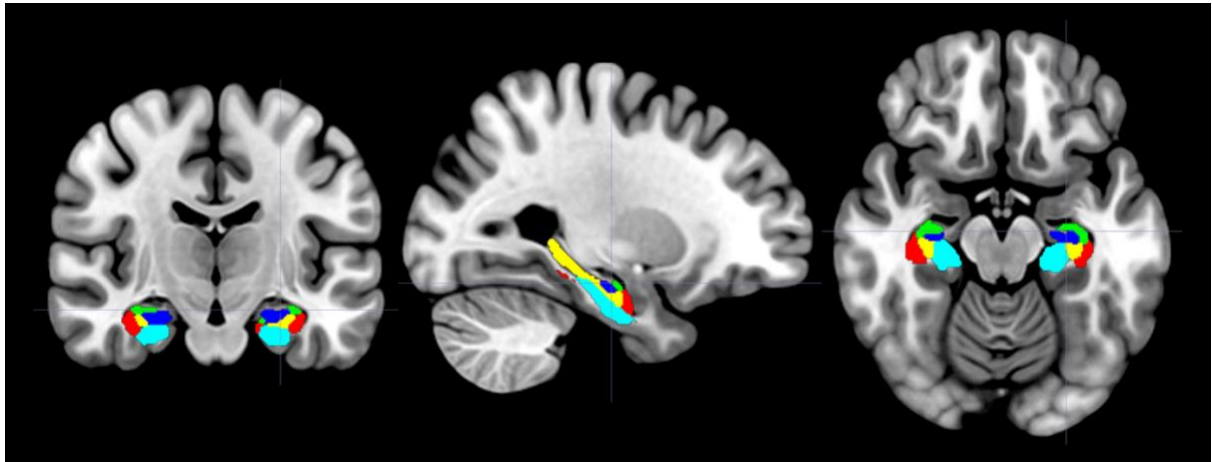
Figure S2. Region-of-interest mask for the hippocampal subfield analysis.

ROI masks for bilateral hippocampal subregions: dentate gyrus (yellow), subiculum (light blue), CA1 (red), CA2 (green), and CA3 (dark blue) displayed on a standard brain template.

Figure S3. Scatterplot of follow-up GAF scores across the total CHR sample with available clinical follow-up (*n*=50).
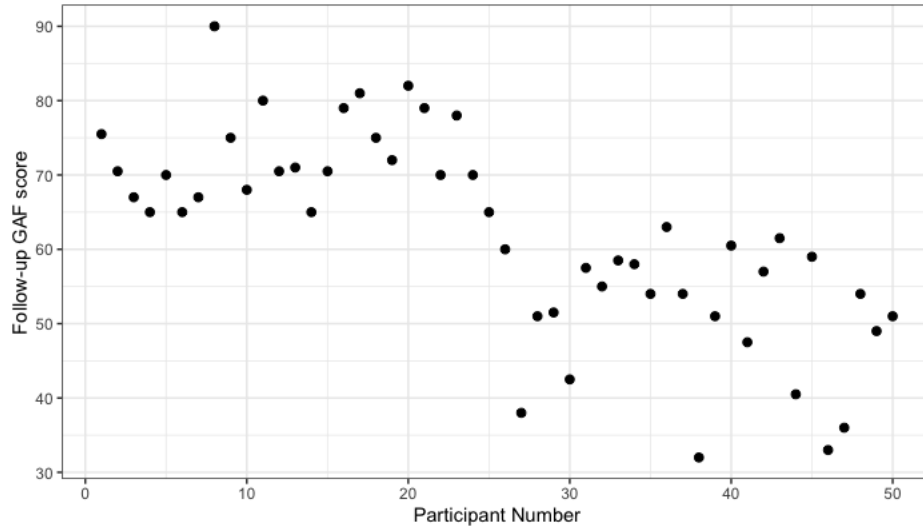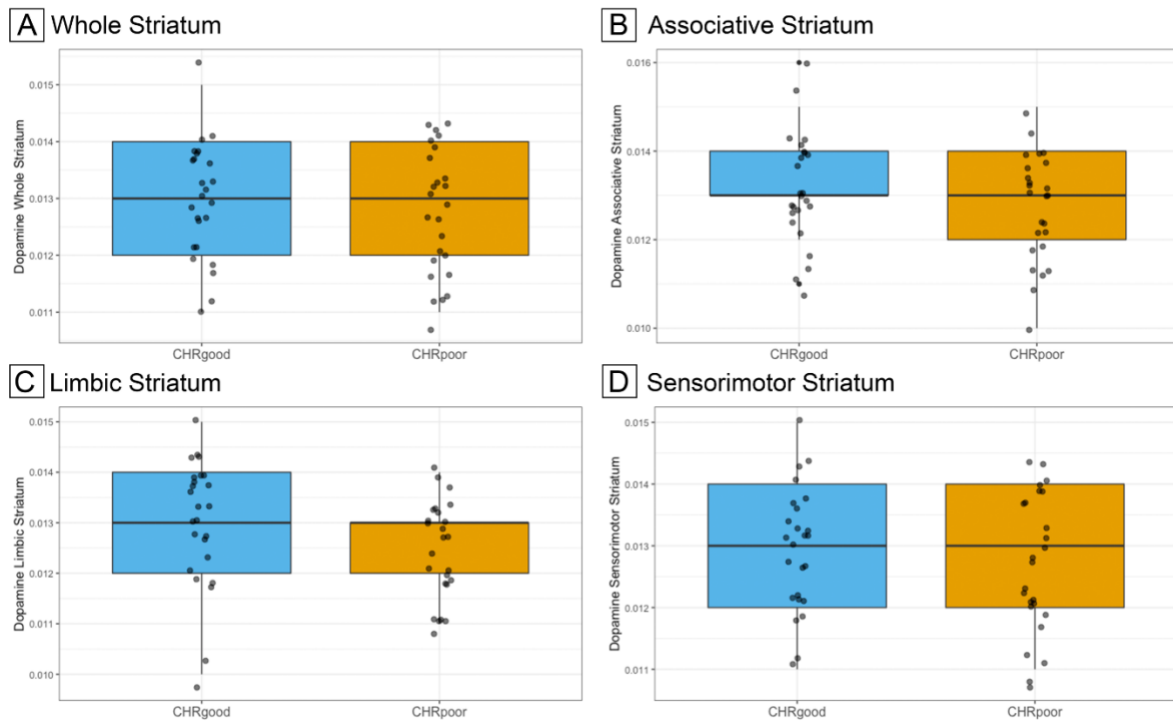
Figure S4. Group differences in dopamine synthesis capacity (whole striatum and its subdivisions) between CHR-Poor (*n*=25) and CHR-Good subgroups (*n*=25).


Boxplots with overlaid individual datapoints for (A) whole, (B) associative, (C) limbic, and (D) sensorimotor striatum. There were no significant differences between CHR individuals with good functional outcomes (blue) and CHR individuals with poor outcomes (orange). Striatal dopamine is quantified in K_i^{cer} min^{-1}.

Figure S5. Group differences in dopamine synthesis capacity (whole striatum and its subdivisions) between HC (*n*=28) and the total CHR sample (*n*=67).
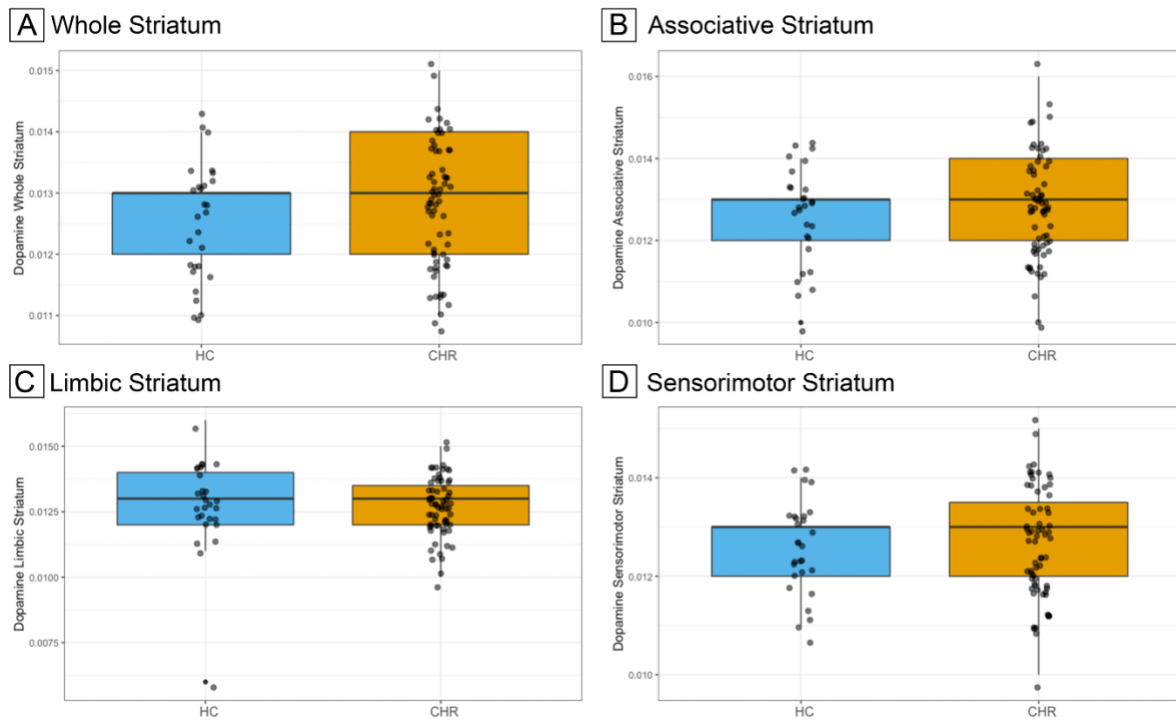
Boxplots with overlaid individual datapoints for (A) whole, (B) associative, (C) limbic, and (D) sensorimotor striatum. There were no significant differences between HC (blue) and the total CHR sample (orange). Striatal dopamine is quantified in K_i^{cer} min^{-1}.

Figure S6. Associations between hippocampal rCBF and dopamine synthesis capacity in striatal subdivisions in CHR individuals with poor functional outcomes compared to those with good outcomes.
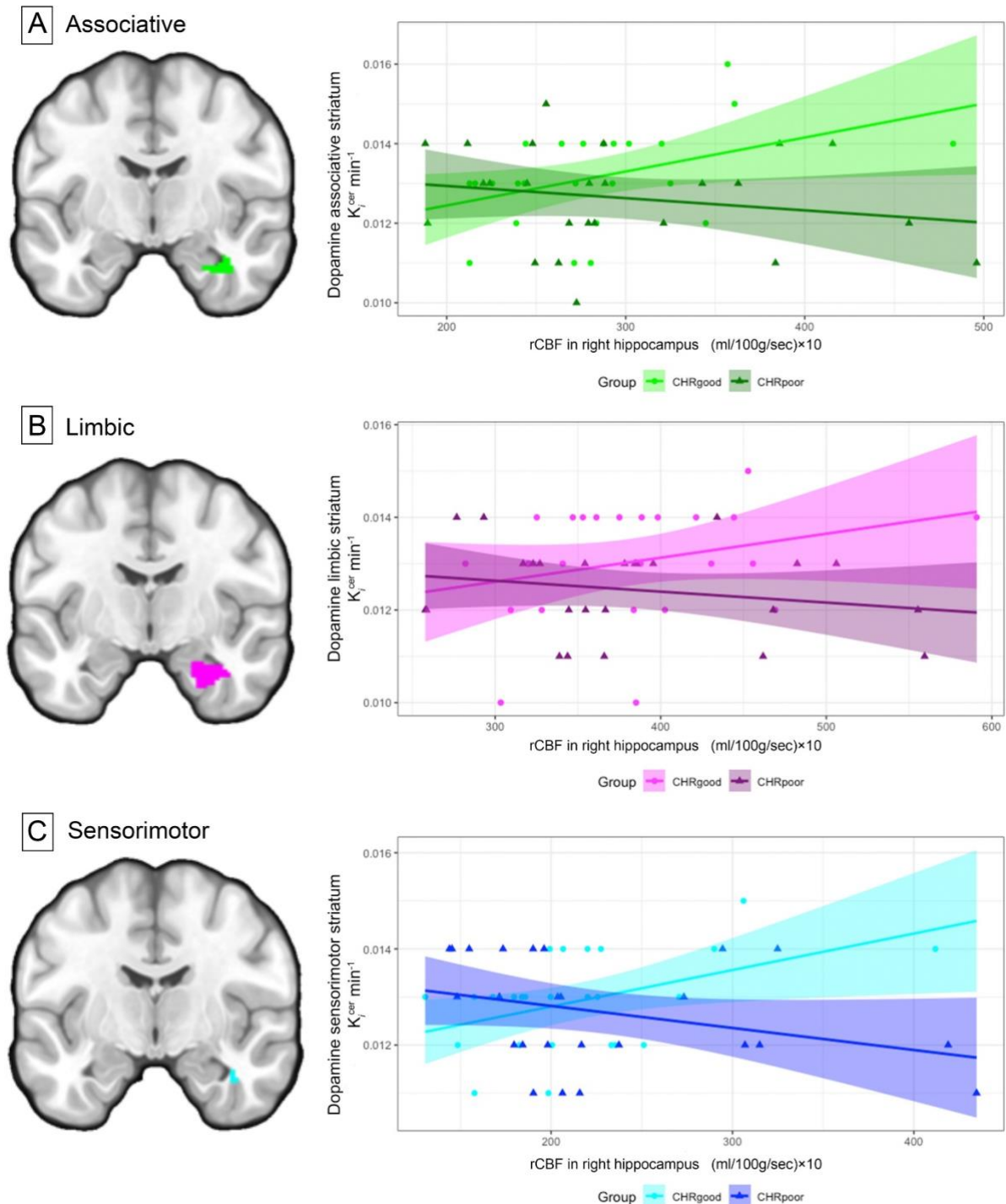
Significant hippocampal rCBF x K_i interaction effects for (A) associative (p_{fwe} = 0.046), (B) sensorimotor (p_{fwe} = 0.036), and trend-level in the limbic (p_{fwe} = 0.054) striatum. Cluster-averaged effects are displayed on a standard brain template and corresponding scatterplots of the association with regression line and 95% CI.

References

1   Allen P, Chaddock CA, Egerton A, Howes OD, Bonoldi I, Zelaya F, et al. Resting Hyperperfusion of the Hippocampus, Midbrain, and Basal Ganglia in People at High Risk for Psychosis. The American journal of psychiatry. 2016;173(4):392-9.

2   Allen P, Azis M, Modinos G, Bossong MG, Bonoldi I, Samson C, et al. Increased Resting Hippocampal and Basal Ganglia Perfusion in People at Ultra High Risk for Psychosis: Replication in a Second Cohort. Schizophrenia bulletin. 2018;44(6):1323-31.

3   Williams DS, Detre JA, Leigh JS, Koretsky AP. Magnetic resonance imaging of perfusion using spin inversion of arterial water. Proceedings of the National Academy of Sciences of the United States of America. 1992;89(1):212-6.

4   Alsop DC, Detre JA, Golay X, Gunther M, Hendrikse J, Hernandez-Garcia L, et al. Recommended implementation of arterial spin-labeled perfusion MRI for clinical applications: A consensus of the ISMRM perfusion study group and the European consortium for ASL in dementia. Magn Reson Med. 2015;73(1):102-16.

5   Buxton RB, Frank LR, Wong EC, Siewert B, Warach S, Edelman RR. A general kinetic model for quantitative perfusion imaging with arterial spin labeling. Magn Reson Med. 1998;40(3):383-96.

6   Egerton A, Chaddock CA, Winton-Brown TT, Bloomfield MAP, Bhattacharyya S, Allen P, et al. Presynaptic Striatal Dopamine Dysfunction in People at Ultra-high Risk for Psychosis: Findings in a Second Cohort. Biological psychiatry. 2013;74(2):106-12.

7   Howes OD, Bonoldi I, McCutcheon RA, Azis M, Antoniades M, Bossong M, et al. Glutamatergic and dopaminergic function and the relationship to outcome in people at clinical high risk of psychosis: a multi-modal PET-magnetic resonance brain imaging study. Neuropsychopharmacology : official publication of the American College of Neuropsychopharmacology. 2020;45(4):641-48.

8   Bloomfield MA, Pepper F, Egerton A, Demjaha A, Tomasi G, Mouchlianitis E, et al. Dopamine function in cigarette smokers: an [(1)(8)F]-DOPA PET study. Neuropsychopharmacology : official publication of the American College of Neuropsychopharmacology. 2014;39(10):2397-404.

9   Montgomery AJ, Thielemans K, Mehta MA, Turkheimer F, Mustafovic S, Grasby PM. Correction of head movement on PET studies: comparison of methods. J Nucl Med. 2006;47(12):1936-44.

10   Jauhar S, Veronese M, Rogdaki M, Bloomfield M, Natesan S, Turkheimer F, et al. Regulation of dopaminergic function: an [(18)F]-DOPA PET apomorphine challenge study in humans. Transl Psychiatry. 2017;7(2):e1027.

11   Martinez D, Slifstein M, Broft A, Mawlawi O, Hwang DR, Huang Y, et al. Imaging human mesolimbic dopamine transmission with positron emission tomography. Part II: amphetamine-induced dopamine release in the functional subdivisions of the striatum. Journal of cerebral blood flow and metabolism : official journal of the International Society of Cerebral Blood Flow and Metabolism. 2003;23(3):285-300.

12   Schobel SA, Chaudhury NH, Khan UA, Paniagua B, Styner MA, Asllani I, et al. Imaging patients with psychosis and a mouse model establishes a spreading pattern of hippocampal dysfunction and implicates glutamate as a driver. Neuron. 2013;78(1):81-93.

13   Schobel SA, Lewandowski NM, Corcoran CM, Moore H, Brown T, Malaspina D, et al. Differential targeting of the CA1 subfield of the hippocampal formation by schizophrenia and related psychotic disorders. Archives of general psychiatry. 2009;66(9):938-46.

14   Lieberman JA, Girgis RR, Brucato G, Moore H, Provenzano F, Kegeles L, et al. Hippocampal dysfunction in the pathophysiology of schizophrenia: a selective review and hypothesis for early detection and intervention. Molecular psychiatry. 2018;23(8):1764-72.

15   Amunts K, Kedo O, Kindler M, Pieperhoff P, Mohlberg H, Shah NJ, et al. Cytoarchitectonic mapping of the human amygdala, hippocampal region and entorhinal cortex: intersubject variability and probability maps. Anat Embryol (Berl). 2005;210(5-6):343-52.

16   Eickhoff SB, Stephan KE, Mohlberg H, Grefkes C, Fink GR, Amunts K, et al. A new SPM toolbox for combining probabilistic cytoarchitectonic maps and functional imaging data. NeuroImage. 2005;25(4):1325-35.

17   Egerton A, Stone JM, Chaddock CA, Barker GJ, Bonoldi I, Howard RM, et al. Relationship Between Brain Glutamate Levels and Clinical Outcome in Individuals at Ultra High Risk of Psychosis. Neuropsychopharmacology : official publication of the American College of Neuropsychopharmacology. 2014.

18   Yung AR, Yuen HP, McGorry PD, Phillips LJ, Kelly D, Dell'Olio M, et al. Mapping the onset of psychosis: the Comprehensive Assessment of At-Risk Mental States. The Australian and New Zealand journal of psychiatry. 2005;39(11-12):964-71.